Hyperspectral and panchromatic image fusion through an improved ratio enhancement

Qizhi Xu,[a,b] Weixing Qiu,[a,b] Bo Li,[a,b,*] and Feng Gao[c]

[a]Beihang University, State Key Lab of Virtual Reality Technologies and Systems, Beijing, China
[b]Beihang University, Beijing Key Lab of Digital Media, School of Computer Science and Engineering, Beijing, China
[c]Ocean University of China, Department of Computer Science and Technology, Qingdao, China

Abstract. The goal of ratio enhancement for hyperspectral (HS) image pansharpening is to obtain an enhancement ratio between a simulated low-resolution panchromatic (Pan) image and an original high-resolution Pan image. However, the simulated low-resolution Pan image often suffers from gray-level distortion. To solve these problems, the original HS bands are synthesized to a smaller number of reduced HS bands, then the pixels of Pan and HS images are divided into different groups according to the linearity between the Pan band and the reduced bands. For each pixel group, a nonnegative least-squares algorithm is utilized to calculate the weights of reduced HS bands, so that the simulated Pan image is obtained by weighted summation of reduced HS bands. Finally, the HS image is sharpened by a ratio enhancement. The experiments demonstrated that the proposed method had a good performance on fusion quality.
 [DOI: 10.1117/1.JRS.11.015017]

Keywords: image fusion; remote sensing; hyperspectral image; ratio enhancement; pansharpening.

Paper 16697 received Sep. 23, 2016; accepted for publication Feb. 16, 2017; published online Mar. 8, 2017.

1 Introduction

Some space-borne platforms, such as NASA's Earth observing-1 (EO-1) satellite and China's first target vehicle Tiangong-1 (TG-1), simultaneously acquire both panchromatic (Pan) and hyperspectral (HS) imagery. Due to the incoming radiation energy to imaging sensors and the data volume collected by imaging sensors, a fundamental trade-off between spatial and spectral resolutions has to be made in sensor design.[1] As a consequence, Pan imagery has a high spatial resolution with a broader wavelength range, whereas each band of HS imagery covers a narrower spectral range with relatively poor spatial resolution.[2] However, the HS imagery with the best possible spatial resolution is more desirable to detect spectral and spatial features on the Earth's surface for most remote sensing applications. In order to extend the application potential of HS imagery, an effective image fusion technique is needed to sharpen HS imagery by injecting the geometric detail of Pan imagery to HS imagery.

To date, there have been only a few methods focused on Pan and HS image fusions (see Ref. 3), and most of them are model-based methods: (1) the multiresolution analysis model combines both nonlinear dimensionality reduction and multiresolution analysis fusion to enhance the spatial resolution of a HS image;[4,5] (2) the variational model regards the spatial and spectral quality balance of fused images to be an energy minimization problem;[6,7] and (3) the nonnegative matrix factorization (NMF)-based model decomposes the HS image into basis and weight, then sharpens the basis with the Pan image.[8–10] In general, these methods were shown to achieve a good performance on spectral quality, but the spatial quality often cannot fulfill user expectation. Moreover, because iterative algorithms are involved in the implementations, these methods are computationally expensive in applications.

*Address all correspondence to: Bo Li, E-mail: boli@buaa.edu.cn

1931-3195/2017/$25.00 © 2017 SPIE

On the other hand, a large number of pansharpening techniques are directly designed for multispectral (MS) images rather than HS images.[11–27] According to the differences of original ideas, most of these methods can be divided into three categories, i.e., component substitution (CS) methods, spatial-frequency correction (SFC) methods, and ratioing methods. The CS methods[11–16] use matrix transformations, such as the intensity hue saturation, the principal component analysis, or the Gram–Schmidt (GS) transformations, to project the gray values of an MS image into a new space, and then totally or partially replace a structural component of MS bands in the new space by Pan image in order to sharpen the MS bands. The SFC methods[17–23] use spatial-frequency related transformations, such as wavelet, contourlet, or Laplace transformations, to decompose Pan and MS images into different spatial-frequency scales. For each MS band, the high-frequency components are replaced with components from the Pan image. The fused images are then obtained via an inverse transformation of the modified spectra. The ratioing methods[24–27] utilize image division to obtain an enhancement ratio, and then multiply the ratio with an MS image to obtain a sharpened MS image.

In principle, the three categories of fusion methods inherited from MS pansharpening may be extended to sharpen HS imagery. However, HS imagery pansharpening is more difficult than that of MS imagery. Generally, extending SFC and CS methods to pansharpen k HS images will result in a considerable increase of the computational load and complexity. First, because of the huge number of HS bands, it is too complicated for SFC methods to sharpen HS images based on local context.[28] Second, due to the fact that too many HS bands are involved in a multiple regression[16] to calculate the weights of HS bands, it is difficult for CS methods to synthesize a simulated low-resolution Pan band. Third, and more importantly, the CS methods and SFC methods often blur the spatial details of sharpened images due to the two key problems in applications, i.e., "small miss-registration" and "size difference" problems.[29] Fortunately, ratioing methods have a good tolerance to the two problems. Therefore, ratio enhancement is extended to pansharpen HS images in this paper.

In general, the existing ratio enhancement methods had color distortion phenomenon while processing HS images. The causes of this problem are summarized as follows: (i) the relation that exists between Pan and HS bands is nonlinear; (ii) regional variations of Pan and HS images influence the local accuracy of synthesized Pan images; (iii) the multiple linear regression often fails to obtain the accurate weights of HS bands due to too many HS bands; and (iv) the absence of nonnegative constraint while calculating the weights of HS bands makes the synthesized Pan band physically unreliable. The existing methods did not consider the abovementioned problems. Therefore, it cannot be directly used to pansharpen HS images.

To tackle the color distortion problem of HS image pansharpening, an improved ratio enhancement is proposed in this paper. The main contributions of this paper are as follows: first, the HS bands are greatly reduced to a smaller number of reduced bands by an average of neighbor bands; second, according to the linearity between the Pan band and the reduced bands, the pixels of Pan and HS images are classified into different groups; third, for each pixel group, the nonnegative least-squares algorithm[30] is utilized to calculate the weights of reduced HS bands, so that the simulated Pan image can be obtained by weighted summation of reduced HS bands, and an improved enhancement ratio is obtained by image division between the Pan image and the synthesized Pan image.

The remainder of this paper is organized as follows: the proposed method is presented in the next section. In Sec. 3, the experiments that carried on the Pan and HS images acquired by EO-1 and TG-1 satellites are utilized to validate and analyze the performance of the proposed method. Thereafter, the limitations of the proposed method are discussed in Sec. 4. Finally, conclusions are drawn from the experiments regarding the capacity of spectral and spatial fidelities.

2 Proposed Method

The proposed method is designed to fuse the Pan and HS images that are simultaneously acquired by satellite sensors. Moreover, the spectral range of the Pan images is covered by those of the HS bands. Without this assumption, the qualified low-resolution Pan images cannot be synthesized from HS bands. In this section, first, the HS bands are reduced by the average of

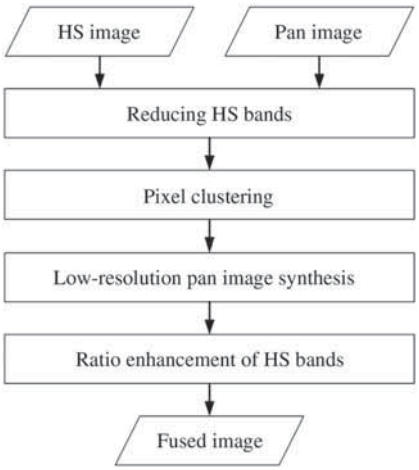

Fig. 1 The processing chart of the proposed method.

neighbor bands. Then, the pixel clustering is performed on the reduced HS bands. Thereafter, the simulated Pan images are synthesized from reduced and classified HS bands, and finally the HS images are pansharpened by ratio enhancement, see Fig. 1.

2.1 *Reducing HS Bands*

The major reason for reducing the HS bands is that the multiple linear regression often fails to obtain the accurate weights of HS bands while there are too many HS bands. Furthermore, the weight calculation will be time consuming if a huge number of bands is involved in multiple linear regression. Therefore, reduction in spectral dimensionality is first applied to the HS bands before synthesizing low-resolution Pan images. To accomplish this task, we have considered the following aspects: (i) select the HS bands involved in reduction, (ii) design the method for reducing the HS bands, and (iii) determine the number of the HS bands after band reduction.

In general, an HS imaging sensor collects images with a spectral interval of 10 nm in the visible to short-wave infrared (SWIR) wavelength ranges, such that an HS data cube has hundreds of spectral bands. However, as pointed out in Ref. 26, only the HS bands whose wavelength ranges are overlapped by that of the Pan band (called overlapped bands) are included to synthesize a low-resolution Pan image. The reason for the selection of the overlapped bands is to generate a simulated Pan image whose pixel value can perfectly approximate that of the high-resolution Pan image. Hence, the sharpened image will obtain good spectral fidelity.

Differently from MS sensors, HS sensors capture narrow spectral bands over a continuous spectral range. In this situation, the pixel values between neighbor HS bands are very similar. This implies that the neighbor HS bands with similar pixel values have similar weight to the contribution of Pan synthesis. Consequently, the number of HS bands can be reduced to a smaller number of synthesized bands by an average of neighbor bands. Assume that the overlapped bands are divided into S groups, and each group has α bands. Generally, the multiple linear regression can reliably obtain the weights of HS bands when $7 \leq S \leq 10$ and $3 \leq \alpha \leq 5$. For ease of understanding, the k'th group of HS bands is written as $b_{k,1}, b_{k,2}, \ldots b_{k,\alpha}$, where $1 \leq k \leq S$. Then, the k'th reduced band (denoted by $\bar{b}_k$) for the k'th group is expressed as

$$d_k = \frac{1}{\alpha} \sum_{t=1}^{\alpha} b_{k,t}. \tag{1}$$

In most cases, the distribution of pixel values varies greatly between the reduced HS bands and the Pan band. This difference makes the reduced HS bands unequally contribute to the synthesized Pan image, and consequently make the enhancement ratio fail to represent the spectral characteristics of the original HS image.[26] Therefore, it is necessary to adjust the gray value of the Pan band and the reduced HS bands before the construction of the synthesized

Pan image. In the proposed method, the means and standard deviations of the Pan band and the reduced HS bands are, respectively, adjusted to the same values, so that every reduced HS band has a balanced contribution to the synthesized Pan image.[27] Before adjusting pixel values, the reduced HS image is extended to the same ground sampling distance (GSD) as the Pan image by bilinear interpolation. Assume that the Pan band is the $(S+1)$'th band, whereas the other S bands are the reduced HS bands. This adjusting scheme is listed as follows:

- Step 1: Calculate the means (A^k), the standard deviations (D^k), the m'th percentile (B^k) and the $(100-m)$'th percentile (E^k) of the k'th band, where $k = 1,2,\ldots,S+1$, and m can be set to 1 or 2, though $m = 1$ is the best option.
- Step 2: Compute the common mean ($\overline{A}$) and standard deviation ($\overline{D}$) according to the following equations:

$$\overline{A} = [\max(B^1 + E^1, \ldots, B^{S+1} + E^{S+1})]/2$$
$$\overline{D} = \max(D^1, \ldots, D^{S+1})(1 + m/100)$$

- Step 3: Adjust the pixel values of the $S+1$ bands by Eq. (2), where x^k is the original pixel value of the k'th band, and y^k is the adjusted value.

$$y^k = \overline{A} + \frac{\overline{D}}{D^k}(x^k - A^k). \tag{2}$$

The adjusted Pan band is denoted by $\bar{P}$, and the adjusted HS bands are denoted by $\bar{b}_k$, where $1 \le k \le S$. Here, the reduced HS bands and the Pan band are simultaneously adjusted. The main reason is to avoid introducing an offset term in the synthesized Pan band. Generally, the synthesized Pan band is often regarded as a summation of weighted HS bands and an offset term.[16] However, it is difficult to calculate the accurate value of the offset term while there are too many HS bands involved, see Eq. (5). Therefore, the means and standard deviations of the Pan band and the reduced HS bands are adjusted to the same values in the proposed scheme.

2.2 *Pixel Clustering*

Because the relation that exists between Pan and HS bands is not linear, moreover, regional variations of Pan and HS images locally influence the accuracy of synthesized Pan images, the low-resolution Pan image with different land covers cannot be globally approximated by a weighted summation of reduced HS bands. To solve this problem, the Pan and reduced HS images are classified into different pixel groups by a k-means algorithm. Note that some existing methods have utilized context-driven schemes, which are based on local context of the images being fused, to eliminate the effect of regional variations. However, it is difficult to enumerate all the contexts in a real-world application. Therefore, color distortion emerges in the case that the contexts are different from the assumption of context-driven schemes.

In order to solve these problems, the images are classified according to the correlation between the adjusted Pan band and the adjusted HS bands. The reason for the selection of a correlation-based clustering is that the good correlation of the pixels within each class indicates a good linear relation between the adjusted Pan band and the adjusted HS bands, so that the synthesized Pan image can be obtained by a weighted summation of adjusted HS bands. In this situation, all the pixels that are clustered by correlation can consequently use the same weight vector while generating the synthesized Pan image. Let $\mathbf{v_j} = [\bar{b}_1(j), \bar{b}_2(j), \ldots, \bar{b}_S(j), \overline{P}(j)]$ be the pixel value of the adjusted Pan and HS bands, where j is the pixel index. In addition, let μ_t be the component-wise mean of the pixels in the category C_t. Then the images are divided by the k-means algorithm that aims at minimizing the objective function as

$$F = \sum_{t=1}^{N}\sum_{j\in C_t} \mathrm{dist}(\mathbf{v_j}, C_t) = \sum_{t=1}^{N}\sum_{j\in C_t}\left[1 - \frac{(\mathbf{v_j} - \bar{v}_j)(\mu_t - \bar{\mu}_t)}{|\mathbf{v_j} - \bar{v}_j||\mu_t - \bar{\mu}_t|}\right], \tag{3}$$

where $\bar{v}_j$ and $\bar{\mu}_t$ are, respectively, the means of the vectors v_j and μ_t for centering and normalizing those vectors to zero mean and unit standard deviation, and N is the number of classified categories.

Note that N is a key parameter for the proposed method to obtain a good spectral fidelity. We have performed the experiments using the data sets with different land covers. The data sets included five pairs of Pan and HS images from the EO-1 satellite and five pairs of Pan and HS images from the TG-1 vehicle platform. The following results were obtained from this experiment: (i) when $N = 2$, the proposed method was capable of synthesizing the simulated Pan images with a relatively fast convergence of k-means algorithm, and (ii) when $N > 2$, there are too many small pixel blocks in each pixel group. In this situation, the convergence of the k-means algorithm was much slower. Consequently, N is set to be a constant, i.e., 2, in implementation of this method.

2.3 *Low-Resolution Pan Image Synthesis*

As shown in Sec. 2.1, we have S adjusted HS bands. We denote the k'th adjusted band in category C_t with pixel index j as $\bar{b}_k(j)|j \in C_t$ and the weight of the k'th adjusted band in category C_t as ϕ_t^k, then the adjusted Pan image ($\bar{P}$) for any pixel in category C_t can be expressed as

$$\bar{P}_j^t \approx \sum_{k=1}^{S} \phi_t^k \bar{b}_k(j)|j \in C_t. \tag{4}$$

Because the adjusted Pan band and the adjusted HS bands are adjusted to the same pixel value range in Sec. 2.1, there is no offset term in Eq. (4).

As shown in Ref. 6, the adjusted Pan image is regarded as a linear response of the adjusted HS bands. To be physically realizable, the weight coefficients of adjusted HS bands should be nonnegative. However, the nonnegative constraint is often neglected in the existing methods.[16,27] Any meaningful estimate of ϕ_t^k must comply with nonnegative constraints that make it physically realizable. Therefore, we formulate the nonnegative least-squares problem as

$$\hat{\Phi}_t = \arg\min_{\phi_t > 0} \left| \sum_{j \in C_t} \left[P_j^t - \sum_{k=1}^{S} \phi_t^k \bar{b}_k(j) \right] \right|, \tag{5}$$

where $\Phi_t = [\phi_t^1, \ldots, \phi_t^S]$ and $\hat{\Phi}_t = [\hat{\Phi}_t^1, \ldots, \hat{\Phi}_t^S]$ are the estimated weight coefficients.

For high computational efficiency, the algorithm[30] is used to solve the nonnegative least-squares problem. In the category C_t, the synthesized Pan image is obtained by a weighted summation of the adjusted HS bands, see Eq. (6). The whole synthesized Pan image ($\hat{P}$) is then formed by putting the synthesized image blocks of all the categories together.

$$\hat{P}_j^t = \sum_{k=1}^{S} \hat{\phi}_t^k \bar{b}_k(j)|j \in C_t. \tag{6}$$

It should be noted that the synthesized Pan image can also be introduced into the GS method[15] as the simulated Pan image. However, the GS method is less tolerant to the size difference problem than ratio enhancement.[29] Hence, the ratio enhancement scheme is developed in Sec. 2.4.

2.4 *Ratio Enhancement of HS bands*

After obtaining the synthesized Pan image, the HS bands can be sharpened by multiplying an enhancement ratio, in which the ratio (R) is obtained by image division between the adjusted Pan image ($\bar{P}$) and the synthesized low-resolution image ($\hat{P}$), see Eq. (7). The formula for the sharpening of the k'th HS bands is given in Eq. (8), where b_k and H_k are the k'th HS band and its sharpened result, respectively, whereas (x, y) is the pixel coordinate. Note that b_k is the original HS band,

$$R(x,y) = \bar{P}(x,y)/\hat{P}(x,y), \tag{7}$$

$$H_k(x,y) = R(x,y)b_k(x,y). \tag{8}$$

In this step, although GS transformation can also be employed to perform sharpening, ratio enhancement is the best choice. The reason is that (i) ratio enhancement is much simpler and faster than GS transformation, and (ii) ratio enhancement is more tolerant to small miss-registration and the size difference problem.

3 Experimental Data and Measures

3.1 *Data Sets*

To validate the performance of the proposed method, five pairs of Pan and HS images from the EO-1 satellite and another five pairs of Pan and HS images from the TG-1 platform were used in our experiments. These images have a large coverage of spectral signatures as well as very heterogeneous structures, such as houses, roads, soil, water bodies, and vegetation. The different land covers are useful and necessary to obtain an objective and comprehensive understanding of a pan-sharpening method. For the purpose of clear visualization, only small subsets of experimental images are shown in the demonstrations, see the images in Figs. 2(a) and 2(b). In order to give a convincing demonstration, the subsets that have a variety of land covers are displayed in this paper.

A brief summary of the experimental data sets is listed in Table 1. The EO-1 satellite has two HS sensors; the first sensor detects the wavelength from 400 to 1000 nm of the visible and near

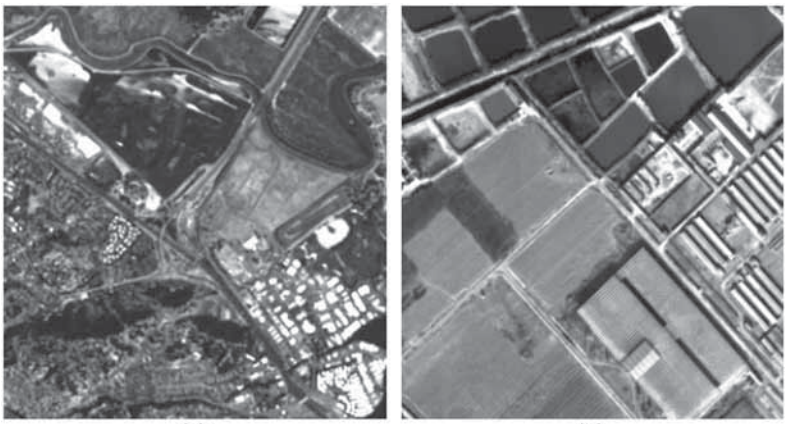

Fig. 2 Subsets (300×320 pixels) of the Pan images used in the experiments. (a) Image from EO-1 data sets and (b) image from TG-1 data sets.

Table 1 An overview of the experimental data sets.

	EO-1		TG-1	
	HS	Pan	HS (VNIR)	Pan
Wavelength (μm)	0.40 to 2.50	0.48 to 0.69	0.40 to 1.00	0.50 to 0.80
GSD (m)	30	10	10	5
Number of bands	242	1	80	1
Study area	San Francisco, Beijing		San Francisco, Beijing	
Digitization	12 bits		12 bits	

infrared (VNIR) range, whereas the second sensor covers the wavelength from 900 to 2500 nm of the SWIR range. Spectral bands 1 to 70 are collected from the VNIR and bands 71 to 242 are collected from the SWIR. To reduce the VNIR/SWIR overlap region, some of these spectral channels are not calibrated and are set to zero; therefore, they were not included in the experiments. Similar to the EO-1 satellite, the TG-1 platform also has VNIR and SWIR sensors. However, the HS images of the SWIR sensors are not available in the experiments. Due to low signal for some channels, only the HS bands 11 to 70 from the TG-1 platform are well calibrated, and the 60 bands are used in the experiments. Before the experiments, the Pan and HS images were coregistered, and then each pair of data sets was cut to the same sizes, i.e., covering an area of 6000×6000 m^2.

3.2 *Measures of Evaluation*

In the experiments, the ground truth of high-resolution HS images is not available. Therefore, we have chosen two different strategies to make a quantitative evaluation. First, we have performed pansharpening on the down-sampled Pan and HS images, and we have then assessed the fusion quality by using the original HS images as Ref. 31. However, the assessments drawn on the down-sampled images may not match user expectation and the concept of quality at full scale.[2] Second, assessments without reference, which are directly obtained on the full scale sharpened images, were consequently included as a necessary complement.[32]

In this paper, the quantitative assessment with reference includes spectral angle mapper (SAM) and ERGAS, whereas the evaluation without reference involves D_λ, D_S, and quality with no reference (QNR). A brief description of these measures is listed as follows:

- SAM[33] is utilized to evaluate the spectral fidelity of sharpened HS images. It calculates the spectral angles between the two spectra $x_r(i,j)$ and $x_f(i,j)$, where $x_r(i,j)$ and $x_f(i,j)$ are the spectra from reference and sharpened images, respectively, and (i,j) is the pixel location. The measure is calculated as

$$\mathrm{SAM} \triangleq \arccos\left[\frac{x_f(i,j)\cdot x_r(i,j)}{|x_f(i,j)||x_r(i,j)|}\right]$$

  A zero angle represents a perfect match of two spectra. In our experimental analysis, SAM is measured by degrees and is averaged for all pixels to yield a global score.
- ERGAS[34] is the French acronym for relative dimensionless global error in synthesis. It evaluates spectral fidelity through root-mean-square error (RMSE) between reference and sharpened HS bands. Hence, the lower the ERGAS value, the better the spectral quality of the merged images. The indicator is defined as

$$\mathrm{ERGAS} \triangleq 100r\sqrt{\frac{1}{N}\sum_{i=1}^{N}\frac{\mathrm{RMSE}^2(i)}{\mathrm{MEAN}^2(i)}},$$

  where r is the spatial resolution ratio between Pan and HS images, N is the number of fused HS bands, and $\mathrm{MEAN}(i)$ is the mean radiance of the i'th spectral band, whereas $\mathrm{RMSE}(i)$ is the RMSE between the i'th reference band and the i'th fused band. As suggested in Ref. 34, the ERGAS value is acceptable when ERGAS < 3.
- D_λ[35] is a measure for spectral fidelity assessment. It is derived from the difference of interband Q values[36] between the fused HS bands and the original HS bands. Let F_i and B_i denote the i'th bands of fused images and original HS images, respectively, then D_λ is written as

$$D_\lambda \triangleq \sqrt{\frac{2}{N^2-N}\sum_{i=1}^{N}\sum_{j=i+1}^{N}|Q(F_i,F_j)-Q(B_i,B_j)|},$$

  where N is the number of fused HS bands. The D_λ measure takes values in [0, 1] with zero being the best value.

Table 2 Average evaluation of sharpened EO-1 HS images produced by different methods.

	SAM	ERGAS	D_λ	D_S	QNR
IGS	4.936	5.91	0.218	0.113	0.694
VM	4.237	5.13	0.196	0.163	0.673
Proposed	**2.180**	**2.69**	**0.101**	**0.095**	**0.814**
MABR	4.218	5.51	0.193	0.111	0.717
NMF	2.254	3.10	0.125	0.156	0.739

Note: The best experimental results are labeled by bold font.

Table 3 Average evaluation of sharpened TG-1 HS images produced by different methods.

	SAM	ERGAS	D_λ	D_S	QNR
IGS	3.811	5.17	0.263	0.101	0.663
VM	2.775	3.90	0.117	0.238	0.672
Proposed	**2.281**	**2.72**	**0.091**	**0.083**	**0.834**
MABR	3.170	4.16	0.126	0.110	0.778
NMF	2.397	3.66	0.098	0.261	0.667

Note: The best experimental results are labelled by bold font.

- D_S[35] is a measure for spatial fidelity assessment. Similar to D_λ and D_s is also derived from the difference of interband Q values.[36] Let P denote a Pan image and $\tilde{P}$ denote a down-sampled version of P, then D_s can be expressed as

$$D_S \triangleq \sqrt{\frac{1}{K}\sum_{i=1}^{K}|Q(F_i,P)-Q(M_i,\tilde{P})|}.$$

  The D_s measure also takes values in [0, 1] with zero being the best value.
- QNR[35] is a combination of D_λ and D_s measures to give an overall assessment of spatial and spectral fidelity. This measure is given by

$$\text{QNR} \triangleq (1-D_\lambda)(1-D_S).$$

QNR takes values in [0, 1] with one being the best value. The main advantage of the QNR index is that the overall evaluation of a fusion product can be assessed at the full scale of a Pan image without reference.

The evaluation of the fusion quality is a complicated work.[37] The quantitative assessment of average evaluation is given in this paper, see Tables 2 and 3. In addition to quantitative assessment, the visual evaluation of sharpened images was also used in the experimental analysis. Because all experimental images are digitalized as 16 bit/pixel, to provide a convincing visual evaluation and analysis result, these images were displayed by the same color mapping tables, which map 16 to 8 bit pixels for visualization.

4 Experimental Results

In order to validate the proposed method, an improved Gram–Schmidt (IGS) method[16] was compared to the proposed method. The IGS method is an improvement of the GS method[15] and has demonstrated good spectral performance for Pan and MS image fusion. In addition, three

recently developed methods, i.e., the similarity measure-based variational method[7] (called VM), the multiresolution analysis and nonlinear PCA band reduction-based method[4] (called MABR method), and the sparse constrained NMF-based method[9] (called NMF method), were also included for experimental analysis. The VM method, MABR method, and NMF method had shown a good performance for HS image pansharpening. A brief description of the four methods and their parameters is given as follows:

1. IGS method: IGS fusion starts with the synthesis of a low-resolution Pan image by multiple regression of HS and Pan images. Then, the GS transformation is applied to the synthesized Pan and the HS bands. Thereafter, the first transformed component is replaced by a high-resolution Pan image. Finally, the sharpened HS bands are generated by an inverse transformation. To avoid the inherent drawbacks, the HS bands whose wavelength ranges are overlapped by that of the Pan band were included to synthesize a low-resolution Pan image in our experiments.
2. VM method: In this method, HS image pansharpening is regarded as an optimization problem, in which a VM was developed under the constraint of spatial and spectral similarity between sharpened images and original images. In the experiments, the distance-based similarity measure was used, and all the parameters of this measure were set to 1, except $\eta = 0.2$ and $\zeta = 2$.
3. MABR method: This method introduces dimensionality reduction of HS images through the nonlinear generalization of standard principal component analysis. The nonlinear principal components were obtained by an auto-associative neural network. The fused HS images were obtained by fusing nonlinear principal components with the PAN images instead of the HS bands.
4. NMF method: In this method, the NMF decomposes the HS image into basis and weight, then sharpens the basis with the Pan image, and finally generates the sharpened HS image by a sparse constrained NMF fusion model. In the experiments, the parameters for the degree of sparsity, sharpening, and spectral preservation are set to 0.01, 0.4, and 0.01, respectively.

4.1 *EO-1 Fusion Results*

Figure 3 is a subset of fusion results of EO-1 data sets, which were acquired over San Francisco in July 23, 2012. The GSD of all the fused images in Fig. 3 is 10 m. To obtain color images of the scene that represent true RGB and color infrared, the bands 16, 23, 29, and 50 were selected. The bands 29, 23, and 16 are used in true RGB display, whereas the bands 50, 23, and 16 are used in color infrared display. In the visual analysis, different band combinations are necessary for subjective evaluation. The HS images of Figs. 3(a) and 3(g) are used as visual reference for evaluating spectral quality, whereas the Pan image of Fig. 2(a) is used as visual reference for evaluating spatial quality.

In true RGB display, it was found that (i) the NMF method and the proposed method had a good performance on spectral fidelity; however, the NMF method produced some spatial artifacts in fused images, and (ii) the IGSmethod, MABR method, and VM method had different color distortions in local regions. The color distortion in the IGS method is mainly because regional variations of Pan and HS images influence the local accuracy of a synthesized Pan image. Because a clustering strategy was designed to tackle this problem, the proposed method avoids color distortion in local regions. In color infrared display, all the methods showed good results on spectral fidelity, but the spatial quality of VM and MABR methods is not as good as that of the other methods.

In addition, quantitative assessments were also provided by calculating the quality measures on the five pairs of EO-1 images. The scores of different methods are listed in Table 2. The GSD of the sharpened HS images for SAM and ERGAS calculations is 30 m, whereas the GSD of the sharpened HS images for D_λ, D_S, and QNR calculations is 10 m. Each score is an average of the quantities obtained from the five pairs of images. In general, these scores are consistent with the visual evaluation. From Table 2, we can find that the scores of the proposed method were better than those of other methods, and the proposed method obtained the best scores for all the measures.

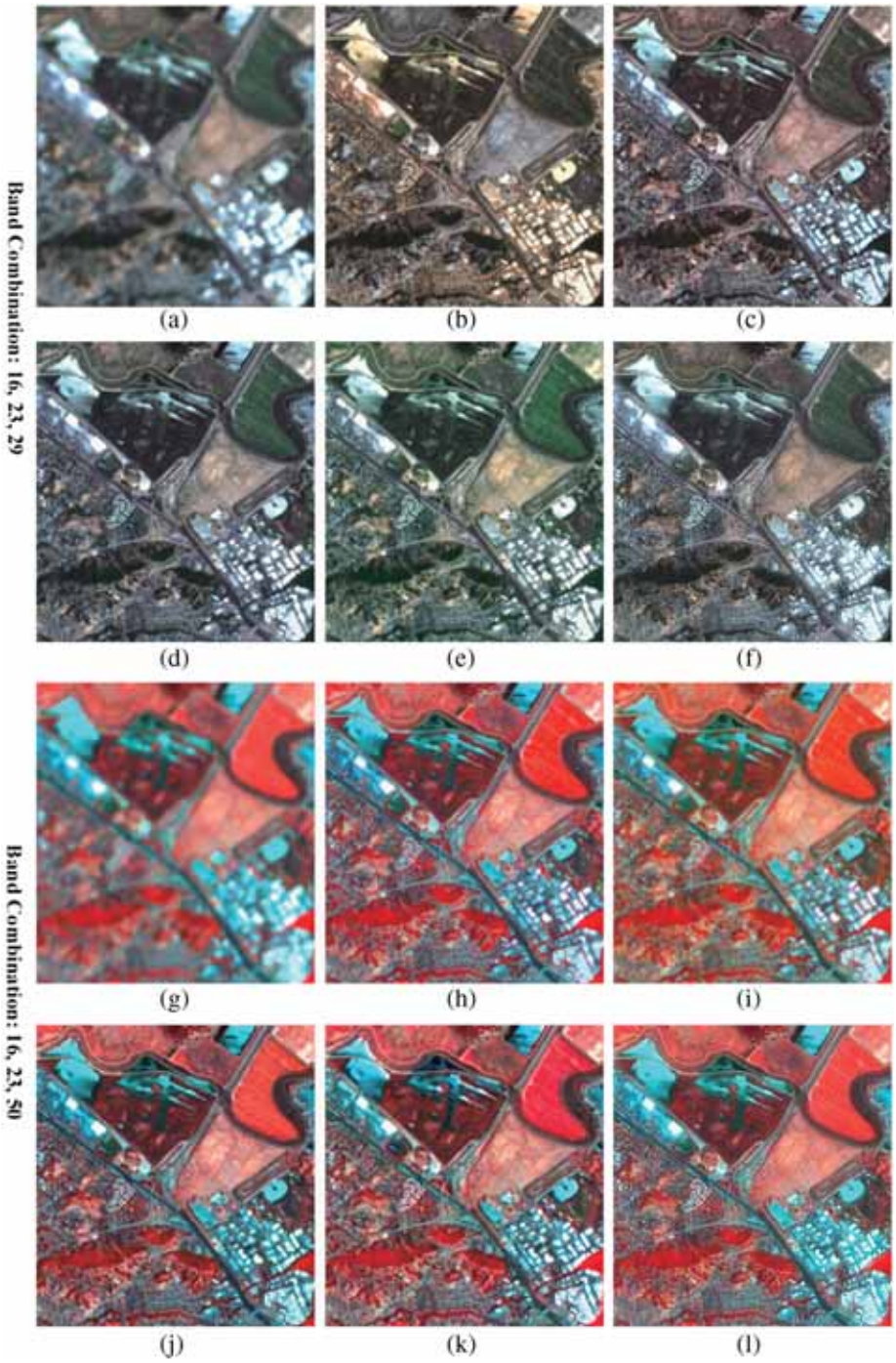

Fig. 3 Subsets (300×320 pixels) of the sharpened EO-1 data sets produced by different methods. (a) HS image, (b) IGS method, (c) VM method, (d) proposed method, (e) MABR method, (f) NMF method, (g) HS image, (h) IGS method, (i) VM method, (j) proposed method, (k) MABR method, and (l) NMF method.

4.2 *TG-1 Fusion Results*

In order to evaluate the fusion algorithms for different sensors, TG-1 data sets were used in the experimental analysis. Because the spatial resolution of TG-1 data sets is higher than that of EO-1 data sets, it is better to give a visual evaluation on the performance of spatial quality. Figure 4 shows a subset of fusion results of TG-1 data sets, which were acquired over Beijing in March

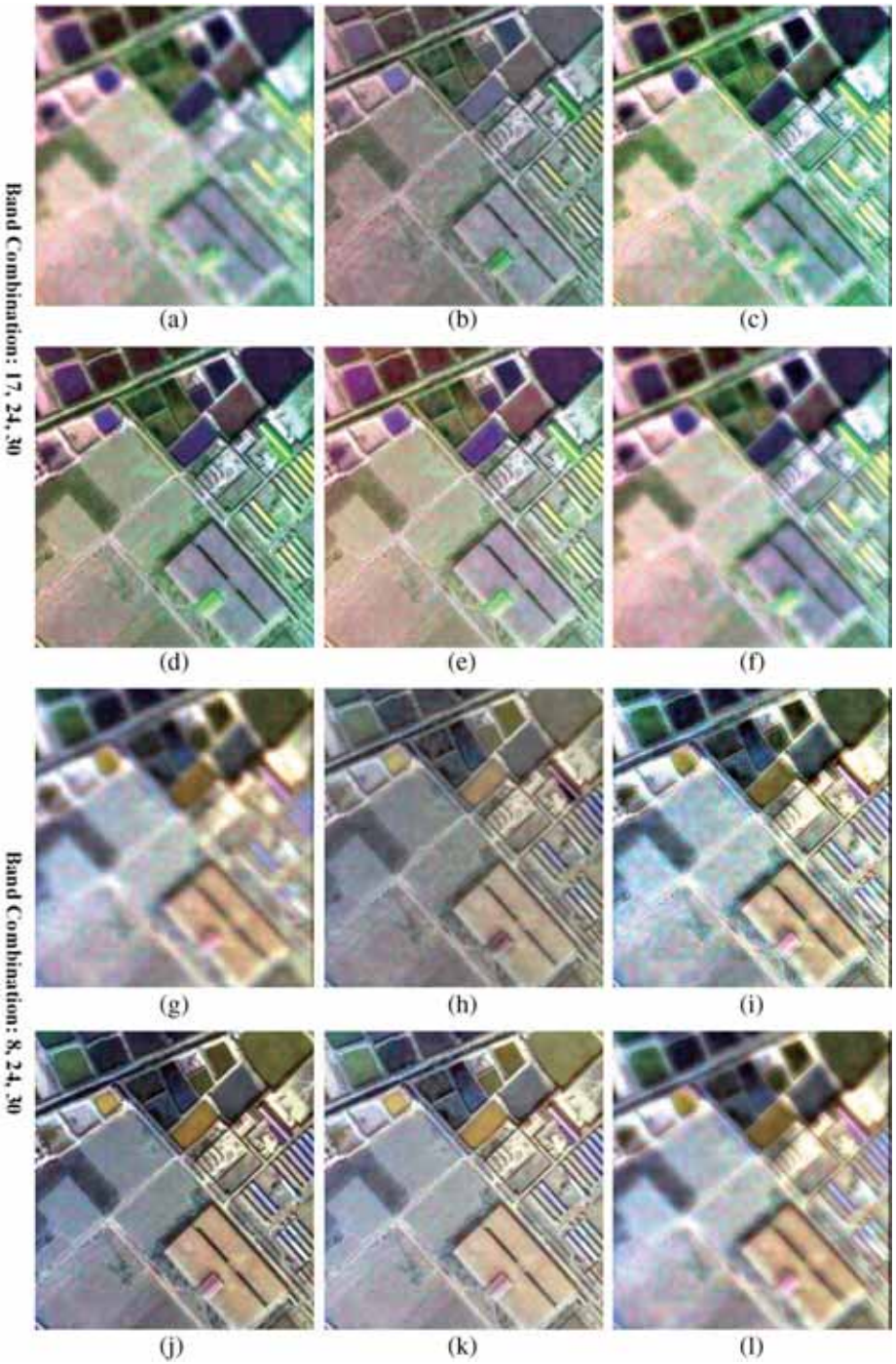

Fig. 4 Subsets (300 × 320 pixels) of the sharpened TG-1 data sets produced by different methods. (a) HS image, (b) IGS method, (c) VM method, (d) proposed method, (e) MABR method, (f) NMF method, (g) HS image, (h) IGS method, (i) VM method, (j) proposed method, (k) MABR method, and (l) NMF method.

29, 2012. The GSD of all the fused images in Fig. 4 is 5 m. The bands 8, 17, 24, and 30 were selected for visual comparison of spectral fidelity, see the original HS images in Figs. 4(a) and 4(g). In addition, the original Pan image is shown in Fig. 2(b), which is used as visual reference for spatial fidelity.

For the two different band combinations in Fig. 4, it was found that NMF and MABR methods had good performance on spectral fidelity, but had poor performance on spatial quality,

Table 4 The average running time (s) for different methods.

	IGS	MABR	VM	NMF	Proposed
EO-1	5.22	14.78	18.21	20.11	8.15
TG-1	4.37	14.25	16.67	23.25	7.23

see Figs. 4(c), 4(f), 4(i), and 4(l). IGS and IR methods had visible color distortion in some local areas, but the spatial quality of the fused images was good, see Figs. 4(b), 4(e), 4(h), and 4(k). The proposed method showed good performance on both spectral and spatial qualities.

Furthermore, quantitative assessments were also provided in Table 3, in which the scores of different methods are mean values of the measures obtained from the five pairs of TG-1 images. The GSD of the sharpened HS images for SAM and ERGAS calculations is 10 m, whereas the GSD of the sharpened HS images for D_λ, D_S, and QNR calculations is 5 m. Generally, these scores are also consistent with the visual evaluation. From Table 3, it was observed that the scores of the proposed method were better than those of other methods, especially for the scores of spatial quality measure D_s. For both EO-1 and TG-1 data sets, the overall performance of the proposed method has exceeded other methods. However, there are some limitations for the proposed method, and we discuss these limitations in Sec. 5.

4.3 *Discussion*

Because the low-resolution Pan image is synthesized through the weighted summation of HS bands, the proposed method is limited to the fusion of simultaneously acquired Pan and HS images. Practically, due to the fact that most of the images are off-nadir and precise coregistration of high-resolution images from different viewing angles is still an unsolved technical problem, it may not be viable to fuse Pan and HS images from two high-resolution satellites.[35] On the other hand, the proposed method is also confined by the overlap constraint, that is, the wavelength range of HS images should cover that of the Pan image. Otherwise, it is physically unreasonable to synthesize a low-resolution Pan image by the weighted summation of HS bands. Fortunately, the Pan and HS sensors that have been carried on the same space platform are designed to meet the overlap constraint in most cases.

In addition, we also found that the computational cost of the proposed method was a little greater than that of the IGS method, but was lower than that of the NMF, MABR, and VM methods. We tested these methods on a high-performance personal computer equipped with an Intel 3.20-GHz central processing unit and 16-GB memory. Table 4 gives the average running time for these methods to pansharpen the EO-1 and TG-1 data sets. The computational efficiency of the proposed method is still needed to improve in future research.

5 Concluding Remarks

This paper has presented a ratio enhancement method for HS image pansharpening, in which the ratio is calculated by image division between a simulated low-resolution Pan image and an original high-resolution Pan image. In the calculation of enhancement ratio, we have developed a scheme that includes the band reduction, image clustering, and nonnegative constraint strategy to tackle the following problems: i.e., nonlinear relation between Pan and HS bands, regional variations of the image being fused, failure of weight calculation due to too many HS bands, and nonnegative restriction of band weights. The experiments on EO-1 and TG-1 data sets demonstrated that the proposed method had good spatial and spectral fidelities.

Acknowledgments

The authors sincerely thank the anonymous referees for their constructive comments. The EO-1 datasets were provided by the United States Geological Survey (http://earthexplorer.usgs.gov), whereas the TG-1 data sets were provided by China Manned Space Agency. This work was supported by the National Natural Science Foundation of China (No. 61672076).

References

1. P. Aplin, P. M. Atkinson, and P. J. Curran, "Fine spatial resolution satellite sensors for the next decade," *Int. J. Remote Sens.* **18**(18), 3873–3881 (1997).
2. C. Thomas et al., "Synthesis of multispectral images to high spatial resolution: a critical review of fusion methods based on remote sensing physics," *IEEE Trans. Geosci. Remote Sens.* **46**(5), 1301–1312 (2008).
3. L. Loncan et al., "Hyperspectral pansharpening: a review," *IEEE Geosci. Remote Sens. Mag.* **3**(3), 27–46 (2015).
4. G. A. Licciardi et al., "Fusion of hyperspectral and panchromatic images using multiresolution analysis and nonlinear PCA band reduction," *EURASIP J. Adv. Signal Process.* **2012**(1), 1–17 (2012).
5. G. Vivone et al., "Multiresolution analysis and component substitution techniques for hyperspectral pansharpening," in *Proc. IEEE Int. Geoscience Remote Sensing Symp.*, pp. 2649–2652 (2014).
6. M. Moeller, T. Wittman, and A. L. Bertozzi, "A variational approach to hyperspectral image fusion," *Proc. SPIE* **7334**, 73341E (2009).
7. Z. Shi, Z. An, and Z. Jiang, "Hyperspectral image fusion by the similarity measure based variational method," *Opt. Eng.* **50**(7), 077006 (2011).
8. Z. An and Z. Shi, "Hyperspectral image fusion by multiplication of spectral constraint and NMF," *Optik* **125**(13), 3150–3158 (2014).
9. Q. Chen, Z. Shi, and Z. An, "Hyperspectral image fusion based on sparse constraint NMF," *Optik* **125**(2), 832–838 (2014).
10. O. Berné et al., "Non-negative matrix factorization pansharpening of hyperspectral data: an application to mid-infrared astronomy," in *Proc. IEEE GRSS Workshop Hyperspectral Image Signal Processing: Evolution Remote Sensing*, pp. 1–4 (2010).
11. T.-M. Tu et al., "A fast intensityhue-saturation fusion technique with spectral adjustment for IKONOS imagery," *IEEE Geosci. Remote Sens. Lett.* **1**(4), 309–312 (2004).
12. M. Choi, "A new intensity-hue-saturation fusion approach to image fusion with a tradeoff parameter," *IEEE Trans. Geosci. Remote Sens.* **44**(6), 1672–1682 (2006).
13. T.-M. Tu et al., "Best tradeoff for high-resolution image fusion to preserve spatial details and minimize color distortion," *IEEE Geosci. Remote Sens. Lett.* **4**(2), 302–306 (2007).
14. V. P. Shah, N. H. Younan, and R. L. King, "An efficient pan-sharpening method via a combined adaptive PCA approach and contourlets," *IEEE Trans. Geosci. Remote Sens.* **46**(5), 1323–1335 (2008).
15. C. A. Laben and B. V. Brower, "Process for enhancing the spatial resolution of multispectral imagery using pan-sharpening," U.S. Patent 6,011,875 (2000).
16. B. Aiazzi, S. Baronti, and M. Selva, "Improving component substitution pansharpening through multivariate regression of MS +Pan data," *IEEE Trans. Geosci. Remote Sens.* **45**(10), 3230–3239 (2007).
17. T. Ranchin and L. Wald, "Fusion of high spatial and spectral resolution images: the ARSIS concept and its implementation," *Photogramm. Eng. Remote Sens.* **66**(1), 49–61 (2000).
18. B. Aiazzi et al., "Context-driven fusion of high spatial and spectral resolution images based on oversampled multiresolution analysis," *IEEE Trans. Geosci. Remote Sens.* **40**(10), 2300–2312 (2002).
19. B. Jin, G. Kim, and N. Cho, "Wavelet-domain satellite image fusion based on a generalized fusion equation," *J. Appl. Remote Sens.* **8**(1), 080599 (2014).
20. U. G. Gangkofner, P. S. Pradhan, and D. W. Holcomb, "Optimizing the high-pass filter addition technique for image fusion," *Photogramm. Eng. Remote Sens.* **74**(9), 1107–1118 (2008).
21. Q. Xu et al., "High-fidelity component substitution pansharpening by the fitting of substitution data," *IEEE Trans. Geosci. Remote Sens.* **52**(11), 7380–7392 (2014).
22. S. Li, X. Kang, and J. Hu, "Image fusion with guided filtering," *IEEE Trans. Image Process.* **22**(7), 2600–2610 (2013).
23. X. Jin et al., "Remote sensing image fusion method in cielab color space using nonsubsampled shearlet transform and pulse coupled neural networks," *J. Appl. Remote Sens.* **10**(2), 025023 (2016).

24. A. R. Gillespie, A. B. Kahle, and R. E. Walker, "Color enhancement of highly correlated images. II. Channel ratio and chromaticity transformation techniques," *Remote Sens. Environ.* **22**, 343–365 (1987).
25. Y. Zhang, "A new merging method and its spectral and spatial effects," *Int. J. Remote Sens.* **20**(10), 2003–2014 (1999).
26. Y. Zhang, "System and method for image fusion," U.S. Patent 7,340,099 (2008).
27. Q. Xu et al., "Pansharpening using regression of classified MS and Pan image to reduce color distortion," *IEEE Geosci. Remote Sens. Lett.* **12**(1), 1–5 (2014).
28. B. Aiazzi et al., "Pansharpening of hyperspectral images: a critical analysis of requirements and assessment on simulated PRISMA data," *Proc. SPIE* **8892**, 889203 (2013).
29. Q. Xu, Y. Zhang, and B. Li, "Recent advances in pansharpening and key problems in applications," *Int. J. Data Image Fusion* **5**(3), 175–195 (2014).
30. V. Franc, V. Hlaváč, and M. Navara, "Sequential coordinate-wise algorithm for the non-negative least squares problem," in *11th Int. Conf. Computer Analysis of Images and Patterns*, Versailles, France, pp. 407–414 (2005).
31. L. Wald, T. Ranchin, and M. Mangolini, "Fusion of satellite images of different spatial resolutions: asessing the quality of resulting images," *Photogramm. Eng. Remote Sens.* **63**(6), 691–699 (1997).
32. Y. Zhang, "Understanding image fusion," *Photogramm. Eng. Remote Sens.* **70**(6), 657–661 (2004).
33. R. H. Yuhas, A. F. H. Goetz, and J.W. Boardman, "Discrimination among semi-arid landscape endmembers using the spectral angle mapper (SAM) algorithm," in *Proc. Summaries 3rd Annual JPL Airborne Geoscience Workshop*, pp. 147–149 (1992).
34. L. Wald, "Quality of high resolution synthesized images: is there a simple criterion?" in *Proc. Int. Conf. Fusion Earth Data*, pp. 99–105 (2000).
35. L. Alparone et al., "Multispectral and panchromatic data fusion assessment without reference," *Photogramm. Eng. Remote Sens.* **74**(2), 193–200 (2008).
36. Z. Wang and A. C. Bovik, "A universal image quality index," *Signal Process. Lett.* **9**(3), 81–84 (2002).
37. Y. Zhang, *Methods for Image Fusion Quality Assessment–A Review, Comparison and Analysis, The International Archives of the Photogrammetry, Remote Sensing and Spatial Information Sciences XXXVII, Part B7, Beijing 2008*, pp. 1101–1109, International Society of Photogrammetry and Remote Sensing (2008).

Qizhi Xu received his PhD in computer science from Beihang University, Beijing, China, in 2013. He is currently an associate professor at Beihang University, Beijing, China. From 2013 to 2015, he worked as a postdoctoral fellow in the Canada Research Chair Laboratory in Advanced Geomatics Image Processing, Department of Geodesy and Geomatics Engineering, University of New Brunswick, Canada.

Weixing Qiu received his BS degree from the National University of Defense Technology, Hunan, China, in 2010. He is currently working toward his PhD in computer science from Beihang University, Beijing, China. His research interests include information fusion, object detection, and image understanding.

Bo Li received his PhD in computer science from Beihang University in 1993. He is a professor of computer science and engineering at Beihang University, the director of Beijing Key Laboratory of Digital Media, and has published over 100 conference and journal papers in diversified research fields including digital video and image compression, video analysis and understanding, remote sensing image fusion, and embedded digital image processing.

Feng Gao is currently a lecturer at the College of Information Science and Engineering, Ocean University of China. He received his BS degree in software engineering from Chongqing University, China, in 2008 and received his PhD in computer science from Beihang University, China, in 2015. His research interests include information fusion, computer vision, and image understanding.